

# Frequency degenerate and nondegenerate two-photon absorption spectra of semiconductor quantum dots

L. A. Padilha,<sup>1,2</sup> J. Fu, D. J. Hagan,\* and E. W. Van Stryland\*<sup>1</sup>*College of Optics & Photonics: CREOL & FPCE, University of Central Florida, 4000 Central Florida Blvd., Orlando, Florida 32816-2700, USA*

C. L. Cesar, L. C. Barbosa, and C. H. B. Cruz

<sup>2</sup>*Instituto de Física “Gleb Wataghin,” Universidade Estadual de Campinas (UNICAMP), 13083-970, Campinas, São Paulo, Brazil*

D. Buso and A. Martucci

*Dipartimento di Ingegneria Meccanica—Settore Materiali, Università di Padova, via Marzolo, 9, I-35131 Padova, Italy*

(Received 25 August 2006; revised manuscript received 8 November 2006; published 20 February 2007)

The frequency degenerate and nondegenerate two-photon absorption (2PA) spectra of direct band gap semiconductor quantum dots are studied. Measuring the spectra for both cases in samples of CdSe and CdTe with different quantum dot sizes and size distributions, we observe that the 2PA spectra and the 2PA coefficient are size dependent, so that smaller dots have smaller 2PA even after taking into account the volume fraction. Theory considering the mixing of the hole bands, in a  $\vec{k}\cdot\vec{p}$  model, explains the data quite well except for the smallest dots. A comparison with the parabolic band approximation is also shown.

DOI: [10.1103/PhysRevB.75.075325](https://doi.org/10.1103/PhysRevB.75.075325)

PACS number(s): 42.65.-k, 78.67.Hc, 73.21.La

## I. INTRODUCTION

Quantum-confined semiconductors, including quantum wells, quantum-wires, and quantum dots (QDs) have been investigated for both the understanding of the physical effects in finite structures and the possibility for applications in several areas.<sup>1,2</sup> For QD's, the band gap and luminescence spectra dependence with the QD size are two of the more interesting properties because it is possible to control these spectra by controlling the QD growth. Recently, using core-shell QDs, it has become possible to not only control the luminescence spectra but also enhance the quantum yield, making QDs good candidates for applications in optical amplifiers.<sup>3</sup> Due to their small size, QDs have a high density of surface states (surface/volume ratio is inversely proportional to the QD size), and these states are localized at the interface between the semiconductor and the matrix. The photo-excited electron trapping on these states is faster than some radiative processes which accelerates the electron-hole recombination process, and hence these confined materials exhibit response times up to three orders of magnitude faster than for bulk semiconductors.<sup>4</sup>

Nonlinear optical (NLO) properties, such as nonlinear refraction and two-photon absorption have also been studied for quantum confined semiconductors, but, unlike the linear optical properties, these NLO processes are not completely understood. The combination of high nonlinear refraction and fast response time could make applications in all-optical switching possible.<sup>5,6</sup> Recently, interest has been directed to the imaginary part of the third-order susceptibility, i.e., two-photon absorption (2PA). High values for 2PA cross sections are desirable for applications in three-dimensional imaging of biological systems, and semiconductor QDs may be useful for such applications.<sup>7-9</sup>

Considering the recent interest for the 2PA process in QDs, in a previous paper we reported the dependence of the

2PA coefficient on the size of nanocrystals of CdTe.<sup>10</sup> We found that the maximum value of the 2PA decreases when the QD size is made smaller for these CdTe samples.<sup>10</sup> This is true even taking into account the reduced volume fraction. In the present paper we report both frequency degenerate (i.e., absorption of two equal energy photons) and nondegenerate 2PA spectral measurements for CdTe and CdSe quantum dots. The spectra show that the 2PA coefficient and cross section become smaller at all wavelengths studied as the QD size is reduced even after taking into account the volume fraction. Previously we showed that a model using the parabolic band approximation can fit the 2PA well for larger QDs (QDs radius  $\sim$  exciton Bohr radius).<sup>10</sup> Schmidt *et al.* have studied the influence of quantum confinement on the degenerate 2PA in CdSe QDs.<sup>11</sup> However, this model cannot explain the behavior of 2PA for QDs with radii less than the exciton Bohr radius. In the present paper, we present a study of the degenerate and nondegenerate 2PA for different sizes of different semiconductor QDs and use a theoretical model for describing the 2PA in semiconductor QDs which describes the observed reduction as the QD size is reduced. Unlike the model previously proposed,<sup>10</sup> in this model, the mixing of the heavy and light holes bands is considered by solving the  $\vec{k}\cdot\vec{p}$  Hamiltonian to first order in  $\vec{k}$ . As expected from previously reported results for linear absorption,<sup>12,13</sup> this model improves the fitting of the 2PA for smaller QDs. However, unlike the parabolic band model, it has no analytical solution and must be solved numerically. The theoretical results indicate that the heavy and light holes band mixing is important in quantum dots and for a more complete description the mixing of the split-off band should also be considered.

## II. TWO-PHOTON ABSORPTION: THE $\vec{k}\cdot\vec{p}$ MODEL

Different theories have been proposed for describing the degenerate 2PA in systems with quantum dots.<sup>10,14,15</sup> A

theory based on the parabolic band approximation has been proposed by Fedorov *et al.*<sup>14</sup> for the degenerate 2PA in direct band gap semiconductor QDs. This simple theory describes the semiconductor structure as four independent bands with constant effective mass and does not consider the band mixing between the light and heavy holes in the valence band.<sup>12,14</sup> Kang *et al.*<sup>15</sup> and Sercel and Vahala<sup>12</sup> have shown that it is important to consider the band mixing for a complete description of the electronic structure and, consequently the linear and nonlinear optical properties in such three-dimensionally confined semiconductors. However, when the band mixing is considered, the two-photon transition rate must be calculated numerically, as opposed to the simpler model which results in analytical expressions for the one and two photon transition oscillator strengths. These calculations depend on the semiconductor properties and the quantum dot size and size distribution.<sup>10,14</sup>

In this section we explain how we use the model based on the  $\vec{k} \cdot \vec{p}$  Hamiltonian<sup>12</sup> for describing the complete spectrum of both the degenerate and nondegenerate 2PA in systems with direct band gap semiconductor QDs. In this model we solve the Kane Hamiltonian<sup>12</sup> for the quantum-confined structure considering the perturbation to first order in  $\vec{k}$  for  $\vec{k} \rightarrow 0$ .

For any system, the 2PA transition rate in the degenerate and nondegenerate cases can be calculated from<sup>16</sup>

$$W_{d,nd}^{(2)} = \frac{2\pi}{\hbar} \sum_{i,f} |M_{f,i}^{d,nd}|^2 \delta(E_f - E_i - \hbar\omega_2 - \hbar\omega_1). \quad (1)$$

For the degenerate case,  $\omega_1 = \omega_2$ . The energies  $E_f$  and  $E_i$  are the energies for the final and initial states, respectively.

From here we calculate the transition rate for the nondegenerate 2PA and later we will generalize the result for the degenerate case simply by setting  $\omega_1 = \omega_2 = \omega$ . The matrix element  $M_{f,i}$ , which gives the oscillator strength of the transition from the state  $i$  to  $f$  for the nondegenerate case is written as<sup>10,16</sup>

$$M_{f,i}^{nd} = \sum_a \frac{H_{2f,a} H_{1a,i}}{E_a - E_i - \hbar\omega_1 - i\hbar\gamma} + \frac{H_{1f,a} H_{2a,i}}{E_a - E_i - \hbar\omega_2 - i\hbar\gamma}, \quad (2)$$

where  $a$  represents the intermediate state and

$$H_j = \frac{e}{mc} \vec{A}_j \cdot \vec{p}, \quad (3)$$

where  $H_{j,f,i} = \langle \Psi_f | H_j | \Psi_i \rangle$ , and  $\gamma$  is the inverse of the lifetime for each intermediate state.

The sum over  $a$  includes all states in the valence and conduction bands. This requires that the 2PA in this model, as in the parabolic band model, is constituted by one intra-band and one interband transition.

To solve Eq. (2), it is necessary to know the eigenstates.

From the model proposed in Ref. 14 the states result from the mixing of all four bands and in general are given by<sup>17</sup>

$$\varphi_{FM\pm}(\vec{r}) = \sum_l A_l j_l(k_{n'l}r) \sum_{J_Z} c_{J_Z m M} Y_l^m(\theta, \phi) |u_{J,J_Z}\rangle, \quad (4)$$

where  $J_Z + m = M$ ,  $c_{J_Z m M}$ 's are Clebsch-Gordon coefficients, and  $|u_{J,J_Z}\rangle$  are the eigenstates of the total Bloch angular momentum at  $k=0$ , i.e., at the bottom of the conduction band or at the top of the valence band.<sup>12</sup>  $F$  is the total angular momentum and both  $F$  and  $M$  are good quantum numbers<sup>12</sup> so that the eigenstates can be divided in subspaces with the same quantum number  $F$ .<sup>12</sup>

The electronic conduction band is separated from the two hole bands by the band gap energy,  $E_g$ , and from the split-off band by  $E_g + \Delta_{SO}$ , where  $\Delta_{SO}$  is the split-off energy. If both energies,  $E_g$  and  $\Delta_{SO}$ , are larger than the separations between the states in the hole bands, we can consider the conduction and split-off bands as remote bands and ignore their mixing, and solving them independently. With this in mind, the only band mixing that has to be considered is that between the light and heavy-hole bands. For a more realistic model it would be necessary to also consider the mixing of these bands with the split-off band, especially for smaller QDs when the separation between states in the valence band is not much smaller than  $\Delta_{SO}$ ; however, this is computationally much more complex.

Excluding the mixing of the split-off and conduction bands the eigenstates for these bands are given by

$$\varphi_{FM\pm}(\vec{r}) = j_l(k_{nl}r) \sum_{J_Z} c_{J_Z m M} Y_l^m(\theta, \phi) |u_{J,J_Z}\rangle, \quad (5)$$

with  $k_{nl}$  being the  $n$ th zero of a spherical Bessel function of order  $l$ . In the subspace  $F=1/2$  there are no heavy-hole states. Then the light-hole states are written in the same way as in Eq. (5), but the Bloch eigenstates need to be switched from  $|u_{\frac{1}{2},J_Z}\rangle$  to  $|u_{\frac{3}{2},J_Z}\rangle$ . For the subspace  $F=3/2$ , the hole bands mix with each other, and the eigenstates are written in the same way as in Eq. (4), but  $k_{n'l}$  is not a zero of any spherical Bessel function. It instead consists of zeros of a linear combination of spherical Bessel functions as given in Ref. 12. In our model, we consider that the eigenstates are zero for spatial regions outside the QDs.

The 2PA oscillator strength for each transition is calculated by using the momentum operator in spherical coordinates.<sup>18</sup> The 2PA transition rate is given by the sum of the oscillator strengths over all the allowed two-photon transitions which is numerically calculated. The 2PA coefficient spectrum is given by

$$\beta_{nd}(x_1, x_2) = \frac{N}{E_g^3} \frac{k^2}{x_1 x_2} \langle W_{nd}^{(2)}(x_1, x_2) \rangle, \quad (6)$$

where  $k$  is a constant used for adjusting the theoretical curve to the experimental data,<sup>10</sup>  $N$  the concentration of QDs in the sample,  $x_i = \frac{\hbar\omega_i}{E_g}$ , and  $\langle W_{nd}^{(2)} \rangle$  is the average of the two-photon transition rate [Eq. (1)] over the QD size distribution, which is considered here as a Gaussian distribution.

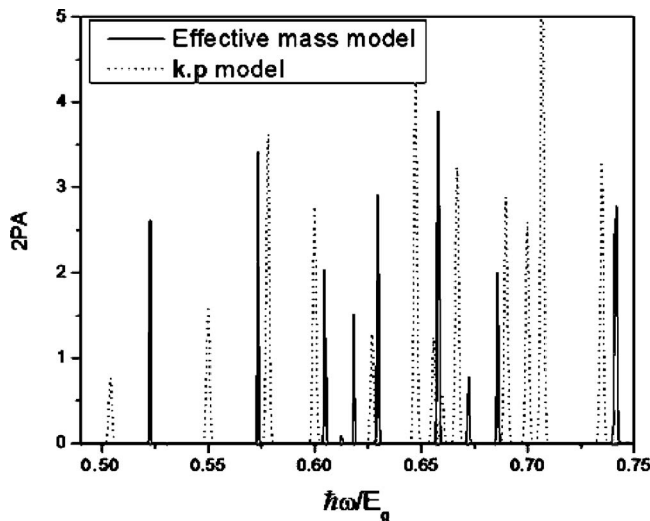


FIG. 1. Comparison between the 2PA transitions predicted by the parabolic band model and the  $\vec{k}\cdot\vec{p}$  approximation for 2.4 nm CdSe QDs.

Figure 1 compares the first 2PA transitions predicted by the parabolic band model<sup>10</sup> and by the  $\vec{k}\cdot\vec{p}$  approximation presented above. The band mixing introduced in this model changes the position of the allowed transitions and also their strength, increasing the relative strength of the high energy transitions.

### III. EXPERIMENTAL

#### A. Synthesis of CdTe and CdSe nanocrystals

The CdTe QDs in borosilicate glass were made by melting the glass matrix components together with CdO and metallic Te, and by heat treating to define the quantum dot size and size distribution. The details of the growth process are described in Ref. 19. Sample CdTe-750 has quantum dots of  $6.6\pm 0.9$  nm radius and a band gap of 1.67 eV. The QD concentration in this sample is  $\sim 0.9\%$ . The second sample, CdTe-600, has smaller nanoparticles,  $3.2\pm 0.4$  nm in radius, and a band gap of 2.07 eV, with a concentration of  $\sim 2.0\%$ . The concentration and size distribution of QDs in each sample is estimated from TEM images. Figure 2(a) shows the linear absorption spectra of these two samples.

The CdSe samples are colloidal QDs dispersed in methanol and octadecene. The synthesis of CdSe quantum dots was realized according to a slightly modified procedure taken from Refs. 20–22. Cadmium oxide (99.99%), selenium (100 mesh, 99.999%), oleic acid (OA), trioctylphosphine (TOP, 97%), ethanolamine (EA), 1-amino-5-pentanol, and 1-octadecene (ODE, tech. 90%) were purchased from Aldrich and were used as received without further purification. A mixture of CdO (0.064 g, 0.5 mmol), OA (1.73 mmol), and ODE (15.78 g) was heated up to 300 °C to allow decomposition of CdO and formation of Cadmium oleate until a clear solution was obtained. A second mixture of Se (0.039 g, 0.5 mmol), trioctylphosphine (0.185 g, 0.5 mmol), and ODE (2.36 g) was heated to 150 °C and kept at constant temperature until a clear yellow solution was observed, indi-

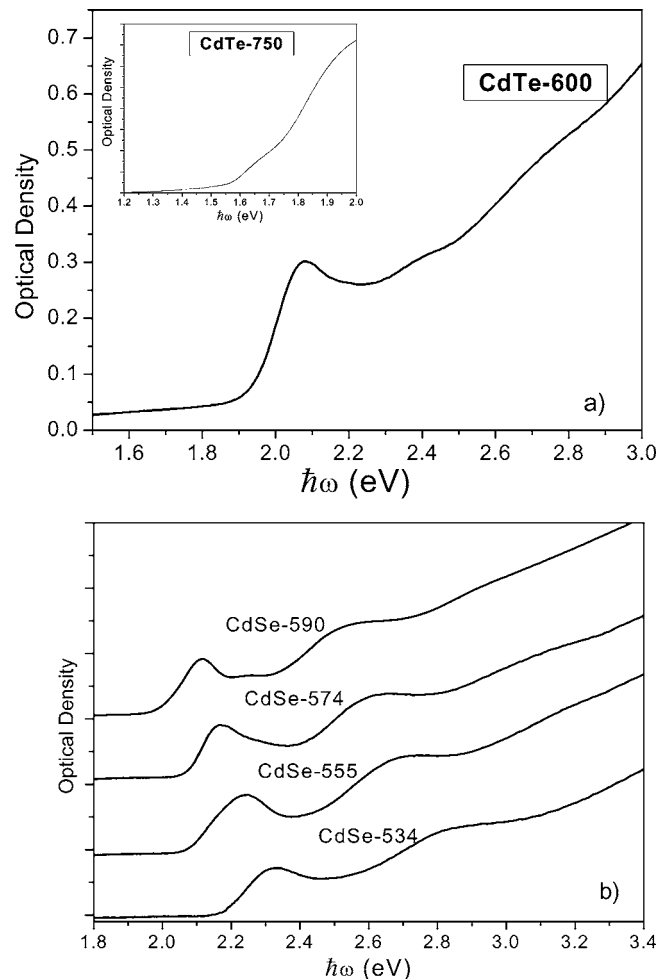


FIG. 2. (a) Linear absorption for the CdTe quantum dots, CdTe 600, inset CdTe 750; (b) Linear absorption for the CdSe quantum dots. The spectra are vertically shifted for clarity.

ating the formation of a TOP-Se complex. The selenium solution was then cooled down to room temperature and rapidly injected into the hot cadmium solution. The temperature of the final mixture was set at 280 °C to allow crystal growth. The solution undergoes a slow change in color from pale yellow to dark wine red, directly indicating CdSe particle formation and growth. The reaction was stopped when the desired nanocrystal size was reached. All the synthesis was carried out under argon atmosphere.

Unreacted cadmium and selenium precursors were separated from the main batch through repeated washing using a  $\text{CHCl}_3/\text{CH}_3\text{OH}$  (1:1) solution, and performing centrifugation at 3000 rpm for 5 min after each wash.

Ethanolamine, EA, was added to the CdSe solution in ODE (EA: superficial Cd atoms=100:1) and incubated overnight until a red deposit was isolated at the flask bottom. Clear ODE was then separated from the main batch and the CdSe powder washed with acetone. To dissolve the nanoparticles into polar solvents such as methanol (MTH), 1-amino-5-pentanol was used to complex the nanocrystal surfaces. The same molar ratio reported for EA has been adopted for the above described capping procedures.

The resulting samples are CdSe-590 (concentration = 5.80 g/L,  $R=2.4\pm 0.5$  nm) dispersed in ODE, CdSe-574

(concentration=4.04 g/L,  $R=2.2\pm 0.5$  nm) dispersed in ODE, CdSe-555 (concentration=4.7 g/L,  $R=2.1\pm 0.3$  nm) dispersed in MTH, and CdSe-534 (concentration=3.5 g/L,  $R=1.9\pm 0.3$  nm) dispersed in MTH. Figure 2(b) shows the linear absorption spectra for the CdSe samples.

For all the CdTe and CdSe samples the QD average sizes were measured directly via TEM microscopy and the linear absorption spectra were taken at room temperature.

### B. Experimental setup

The degenerate 2PA spectra were measured by two different experiments,  $Z$  scan and photoluminescence. The CdTe samples, which are more concentrated but present low quantum yield for photoluminescence, were measured by open aperture  $Z$  scans at many wavelengths.<sup>23</sup> The CdSe samples were measured by two-photon excited luminescence (or two-photon fluorescence, 2PF),<sup>24</sup> because they have low concentration but high quantum yield. Both experiments,  $Z$  scan and 2PF, are performed using an OPA (optical parametric amplifier) tunable from 500 nm up to 2.2  $\mu\text{m}$ , generating femtosecond pulses with  $\sim 140$  fs FWHM, 1 kHz repetition rate. The OPA is pumped by a Clark-MXR CPM-2010, which generates 1 mJ and 140 fs pulses at 775 nm, at 1 kHz repetition rate. The 2PF technique is a relative method to measure 2PA. The absolute 2PA coefficients are obtained by comparing the sample's photoluminescence excitation spectrum with the same spectrum from a reference sample, in this case, Rhodamine 6G.<sup>25</sup>

The nondegenerate 2PA spectra were measured by a femtosecond pump-probe technique with a single wavelength pump and a weak white light continuum (WLC) probe.<sup>26</sup> In this experiment the pump beam is generated by an OPA identical to that used for  $Z$  scan and 2PF measurements, and the WLC probe is generated in a  $\text{CaF}_2$  crystal pumped by another OPA at 1300 nm. Spectral filters, with  $\sim 10$  nm spectral bandwidth and central wavelength at  $\omega_1$ , are used for selecting the probe wavelength so that we are able to study the absorption of the probe photon, with energy  $\hbar\omega_1$ , due to the presence of the pump photon, with energy  $\hbar\omega_2$ . Using filters with different  $\omega_1$  we can cover the entire spectrum for the nondegenerate 2PA. The pump photon energy is chosen to be lower than  $\frac{1}{2}E_g$ , and the probe beam is made weak enough so that the influence of any degenerate 2PA in our nondegenerate experiment is negligible.

## IV. EXPERIMENTAL RESULTS

Figures 3 and 4 show the degenerate 2PA spectra for all the CdTe and CdSe samples studied. The dependence of these spectra with the size of the QDs is clear. The theoretical curves shown for each sample are calculated from the parabolic band approximation.<sup>10</sup> It can be seen that this theory fits the data reasonably well for QDs with radius close to the Bohr radius,  $a_B$ , i.e., CdTe-750 (for CdTe  $a_B \approx 7.5$  nm).

From Figs. 3 and 4 it is clear that the parabolic band approximation<sup>10</sup> fails to describe the 2PA for the smallest quantum dots. This occurs mainly in two regions, close to the

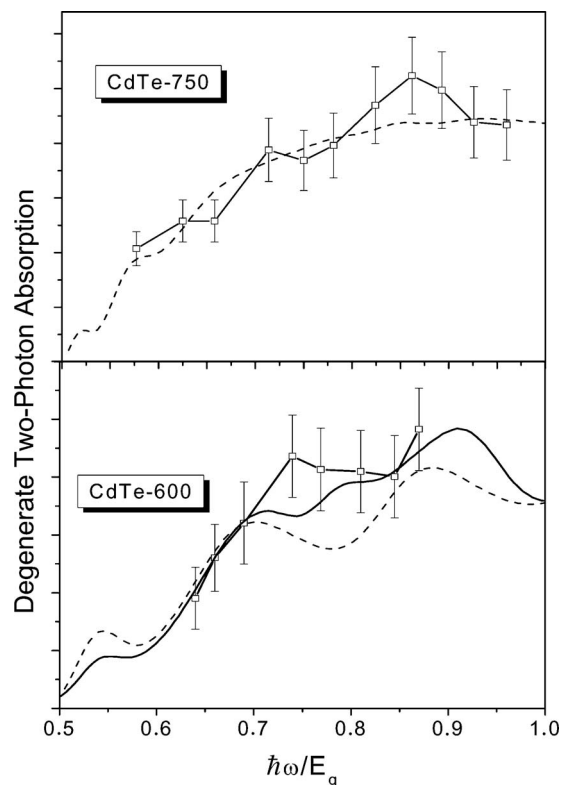


FIG. 3. Degenerate 2PA for CdTe quantum dots. The experimental data is fit by the parabolic band approximation (Ref. 9) (dashed line) and the  $\vec{k}\cdot\vec{p}$  model (continuous line).

2PA edge and for higher photon energies near the linear absorption edge. That theory predicts a first peak that is not experimentally measurable and at higher energies it predicts smaller values for the 2PA than those measured.

The fitting by the model based on the  $\vec{k}\cdot\vec{p}$  Hamiltonian is made for the degenerate 2PA for CdTe-600 and for the four CdSe QD samples, CdTe-750 is not fitted by this model because for this sample the 2PA spectrum involves about 4 times more transitions than the samples with smaller QDs and then the calculation would be very time consuming, also the parabolic band approximation fits well the 2PA for this sample. When band mixing is considered, the first peak's height decreases and for the higher energy spectral region the values predicted are closer to those experimentally measured. The reason for this is that the band mixing breaks the symmetry of the wave functions and allows some transitions that were forbidden in the parabolic band model, thus increasing the oscillator strength at higher energies relative to lower energies. For the parabolic band approximation, the states are proportional to spherical Bessel functions and the eigenvalues are given by the zeros of those functions. Then, due to the orthogonality of the spherical Bessel functions, a transition from the  $n$ th valence state to the  $n'$ th conduction state has as intermediate states only the  $n'$ th valence state and the  $n$ th conduction state.<sup>10,14</sup> From the band mixing, the eigenstates of the hole states are not zeros of the spherical Bessel function, but come from a linear combination of these [see Eq. (4)]. Then the number of intermediate states increases. For example, for the transition from  $4S_{3/2}$  (fourth hole-

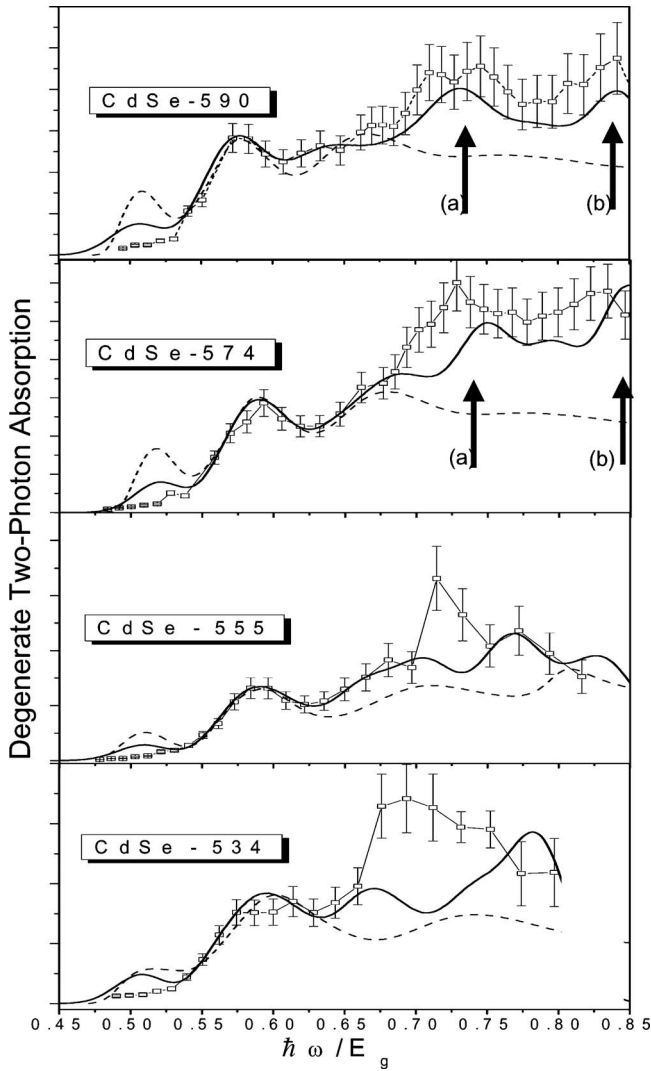


FIG. 4. The same as Fig. 3 but for the CdSe quantum dot samples. The arrows (a) and (b) in the spectra for the two samples with the largest quantum dots show the position of the predicted transitions  $4S_{3/2} \rightarrow 1P_e$  and  $5S_{3/2} \rightarrow 1P_e$ , respectively.

mixing state in the  $F=3/2$  subspace, with odd parity) to  $1P_e$  (first electronic state with odd parity), the intermediate states can be  $1LH_{1/2}^+$ ,  $nP_{3/2}$ ,  $nS_e$ ,  $nD_e$ , with  $n=1, 2, 3, \dots$ , using the same notation as Norris and Bawendi.<sup>27</sup>

Many authors have reported that the band mixing is important for describing linear processes in QDs,<sup>12,14</sup> and our results show the importance for describing the complete 2PA spectrum as well. Even though there is considerable improvement in the fitting over the parabolic band approximation, from Fig. 4, we see that the present theory still fits the larger QDs better than the smallest QDs. The reason may be that this theory does not consider the mixing of the conduction and split-off bands. This approximation is valid if  $E_g$  and  $\Delta_{SO}$  are larger than  $\Delta E$ , the difference between the energies of two states within the valence band.

The difference between the energies of the eigenstates of the QDs is, to first approximation,<sup>12</sup> proportional to the inverse of the QD radius squared ( $R^{-2}$ ).<sup>12,14</sup> Consequently, for

smaller QDs  $\Delta E$  increases becoming comparable to  $E_g$  and  $\Delta$ , and the split-off band can no longer be considered as remote. For the best fitting of the smaller QDs, especially samples CdSe-555 and CdSe-534, it would be necessary to include the mixing of the split-off band. The fittings in Fig. 4 suggest that even for the samples with the largest QDs, an even more complete model, considering the split-off band mixing and going to higher order perturbation in the vector  $\vec{k}$ , may fit the 2PA spectrum better. The peaks in the data for samples CdSe-590 and CdSe-574 (see Fig. 4) are identified from the theory as being due to transitions from the fourth and fifth mixed hole states with odd parity to the first electronic state with odd parity ( $4S_{3/2} \rightarrow 1P_e$  and  $5S_{3/2} \rightarrow 1P_e$ ). The peaks measured are not exactly in the position predicted by the theory; however, the shift of about 2% of the total value may be due to the choice of the fitting parameters.

Figure 5 shows the degenerate and nondegenerate 2PA spectra for CdTe-750, CdTe-600, CdSe-590, and CdSe-555 and the theoretical fitting using the parabolic band approximation for CdTe-750 and the  $\vec{k} \cdot \vec{p}$  model for the other three samples. The parabolic band approximation works well for the largest QDs, CdTe-750, as it close to the bulk semiconductor material. For such large QDs the states are closely spaced and the  $\vec{k} \cdot \vec{p}$  model would be very computationally intense.

The nondegenerate experimental data show enhancement of the 2PA coefficient with respect to the degenerate case since one of the photons has energy closer to  $E_g$  and hence is closer to the intermediate state resonance.<sup>10,24</sup> This is seen in Eq. (2) by the denominators getting smaller from the intraband-interband process. This enhancement is also observed in bulk semiconductors<sup>17</sup> and other materials such as organic dyes.<sup>25</sup>

The degenerate two-photon cross section is calculated by

$$\delta(\omega) = \rho^{-1} \frac{\hbar \omega \beta(\omega)}{N}, \quad (7)$$

and it is given in Goppert-Mayer units ( $1 \text{ GM} = 10^{-50} \text{ cm}^4 \text{ s}^1$ ). Here  $N$  is the QD concentration in the samples and it is given by the volume fraction divided by the single quantum-dot volume. For the nondegenerate two-photon cross section it is necessary to replace  $\omega$  with  $(\omega_1 + \omega_2)/2$  in Eq. (7).  $\rho$  is the local field correction factor, defined by the Maxwell-Garnet model,<sup>28</sup> calculated to be  $\sim 0.3$ . However, in a real sample, because the local field in the quantum dot is reduced, so the useful cross section which is given by  $\frac{\hbar \omega \beta(\omega)}{N}$  instead of Eq. (7). Figure 6 shows the spectrum of the degenerate 2PA cross section for the four CdSe and two CdTe samples. The comparison indicates a decrease of the cross section with a reduction in the QD size even when it is normalized by its volume, but the reduction is more pronounced for the CdTe samples, which have larger difference in size. The same trend has already been shown in water-soluble CdSe by Larson *et al.*<sup>7</sup> and in CdTe quantum dots.<sup>10</sup>

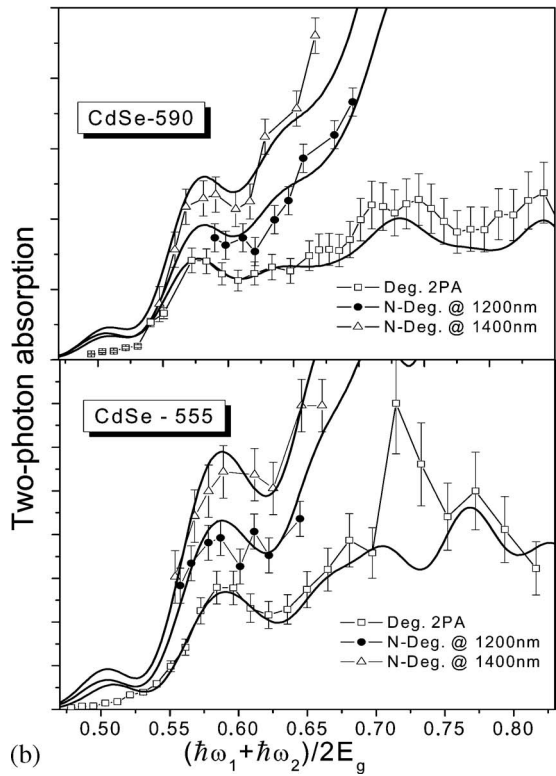
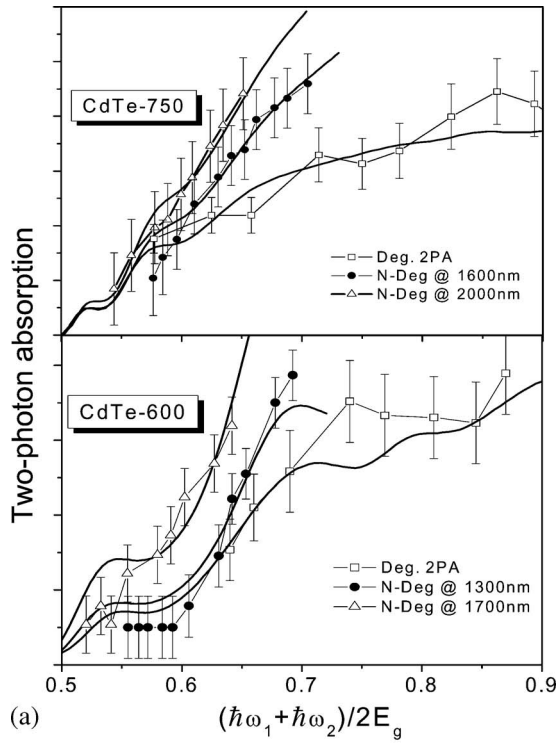


FIG. 5. Nondegenerate 2PA spectra for (a) CdTe and (b) CdSe quantum dot samples. The degenerate spectra are also plotted to show the resonant enhancement. The fitting is done by the parabolic band approximation (Ref. 9) for sample CdTe-750 and by the  $\vec{k}\cdot\vec{p}$  model for all the other 5 samples.

The quantum confinement increases the oscillator strength for each transition separately. However, for the total 2PA cross section it is necessary to consider the sum over all the

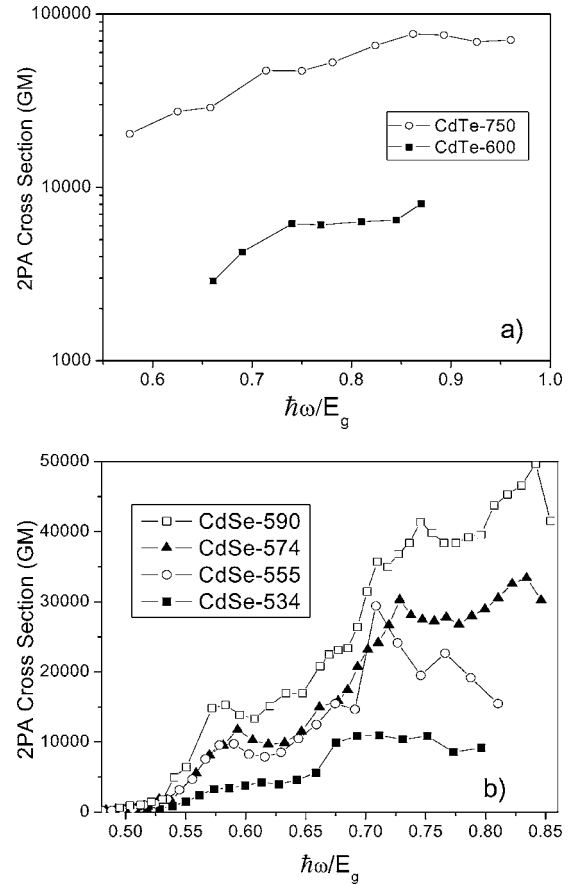


FIG. 6. Degenerate two-photon absorption cross section,  $\delta$  for (a) CdTe (shown on log scale) and (b) CdSe samples. The cross sections shown include the local field correction, as given by Eq. (7).

oscillator strengths of all possible transitions. The energy density of possible transitions decreases as the quantum dots become smaller. Also from Eq. (6), the 2PA is inversely proportional to  $E_g^3$ , and it is well known that the smaller the quantum dot, the larger is the band gap energy.<sup>12,14</sup>

Figure 7 shows the nondegenerate 2PA cross section for CdSe-590 and CdSe-555. The experimental results show the enhancement due to the nondegeneracy and that it is possible to have a two-photon cross section, when considering the local field factor, as high as 60 000 GM for CdSe-590 (2.4 nm in radius) by making the difference between the pump and probe energies larger. From the  $\vec{k}\cdot\vec{p}$  model, we can directly calculate the parameter  $k$  in Eq. (6). This gives  $k \sim 0.296$ , as compared to the best fit values for the data in Fig. 7, which are  $k=0.216$  for CdSe-590 and  $k=0.201$  for all CdSe-555 data. Hence, since the 2PA cross section is proportional to  $k^2$ , our data is in absolute agreement with theory to within a factor of  $\sim 2$ . The theoretical  $\vec{k}\cdot\vec{p}$  fitting agrees well with the experimental data for both samples, predicting the intermediate state resonance enhancement, so this fitting can be extrapolated to even larger differences (e.g., pump at 1700 nm), showing that it is possible to get values even higher for the two-photon cross section far from the linear absorption edge (see dashed lines in Fig. 7).

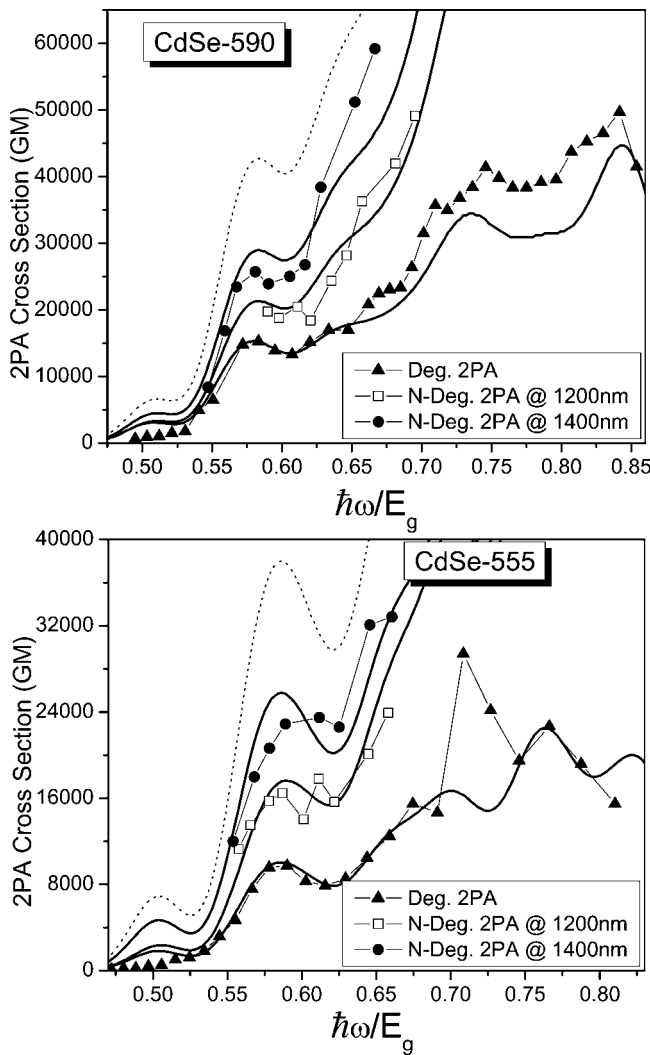


FIG. 7. Enhancement of the two-photon cross section for non-degenerate excitation. The dashed lines show the theoretical prediction for pumping at 1700 nm. The cross-sections shown include the local field correction, as given by Eq. (7).

V. CONCLUSIONS

In this paper we have presented a thorough experimental characterization and analysis of the frequency degenerate and nondegenerate two-photon absorption spectra for different sizes of CdSe and CdTe quantum dots. The influence of

the quantum confinement and of the QD size is clearly observed. For example, the 2PA is reduced for the smaller quantum dots at all wavelengths studied even taking into account the reduced volume fraction. Using two models for describing 2PA in direct band gap semiconductor QDs, in agreement with results observed by using the  $\vec{k}\cdot\vec{p}$  theory for fitting the linear absorption, we show the importance of band mixing in the determination of the 2PA spectra for these QDs. This is especially true for the smaller QDs. The theory proposed, considering the mixing between the light and heavy hole bands obtained from  $\vec{k}\cdot\vec{p}$  theory, fits the data better than the parabolic band approximation, and the improvement comes from breaking the symmetry of the wave functions. From fitting the CdSe QD data, we found that this theory predicted the 2PA spectra better than the parabolic band approximation but added to the complexity. This is especially true for the highest energy transitions we measured as well as for the first band, i.e., that closest to the band edge. However, for the smallest  $\sim 1.9$  nm QDs, i.e., CdSe-534, this theory still did not do a complete job of predicting the 2PA spectrum at the highest energies. For the CdSe samples of intermediate sizes (CdSe-590 and CdSe-574), the experimental data shows evidence of two peaks corresponding to transitions from deeper states,  $4S_{3/2} \rightarrow 1P_e$  and  $5S_{3/2} \rightarrow 1P_e$ , as predicted by the  $\vec{k}\cdot\vec{p}$  model.

The experimental results show an increase of the 2PA due to intermediate-state resonant enhancement when the energy of the two photons is made different, a reduction of the two-photon cross sections with a decrease of the quantum dot average size, and a reduction is observed even if the quantum dot volume is taken into account. However, the maximum measured values for these two-photon cross sections are still higher than 10 000 GM.

ACKNOWLEDGMENTS

L.A.P., C.L.C., L.C.B., and C.H.B.C. gratefully acknowledge CAPES (Coordenação de Aperfeiçoamento de Pessoal de Nível Superior) and FAPESP (Fundação de Amparo à Pesquisa do Estado de São Paulo) for financial support. We also thank the support of the National Science Foundation ECS 0217932, the US Army Research Laboratory W911NF0420012 and the Air Force Office of Scientific Research AFOSR FA95500410200. A.M. thanks MUR-PRIN2006 project 2006031511 for financial support.

\*Also with the Physics Department.

<sup>1</sup>E. H. Sargent, Adv. Mater. (Weinheim, Ger.) 17, 515 (2005).  
<sup>2</sup>N. Finlayson, W. C. Banyai, C. T. Seaton, G. I. Stegeman, M. O'Neill, T. J. Cullen, C. N. Ironside, J. Opt. Soc. Am. B 6, 675 (1989).  
<sup>3</sup>S. V. Kershaw, M. T. Harrison, and M. G. Burt, Philos. Trans. R. Soc. London 361, 331 (2003).  
<sup>4</sup>C. H. B. Cruz, C. L. Cesar, L. C. Barbosa, A. M. de Paula, and S. Tsuda, Appl. Surf. Sci. 110, 30 (1997).

<sup>5</sup>D. Cotter, M. G. Burt, and R. J. Manning, Phys. Rev. Lett. 68, 1200 (1992).  
<sup>6</sup>L. A. Padilha, A. A. R. Neves, E. Rodriguez, C. L. Cesar, L. C. Barbosa, and C. H. B. Cruz, Appl. Phys. Lett. 86, 161111 (2005).  
<sup>7</sup>D. R. Larson, W. R. Zipfel, R. M. Williams, S. W. Clark, M. P. Bruchez, F. W. Wise, and W. W. Webb, Science 30, 1434 (2003).  
<sup>8</sup>X. Gao, Y. Cui, R. M. Levenson, L. W. K. Chung, and S. Nie,

- Nat. Biotechnol. **22**, 969 (2004).
- <sup>9</sup>A. Fontes, K. Ajito, A. A. R. Neves, W. L. Moreira, A. A. de Thomaz, L. C. Barbosa, A. M. de Paula, and C. L. Cesar, Phys. Rev. E **72**, 012903 (2005).
- <sup>10</sup>L. A. Padilha, J. Fu, D. J. Hagan, E. W. Van Stryland, C. L. Cesar, L. C. Barbosa, and C. H. B. Cruz, Opt. Express **85**, 3256 (2004).
- <sup>11</sup>M. E. Schmidt, S. A. Blanton, M. A. Hines, and P. Guyot-Sionnest, Phys. Rev. B **53**, 12629 (1996).
- <sup>12</sup>P. C. Sercel and K. J. Vahala, Phys. Rev. B **42**, 3690 (1990).
- <sup>13</sup>S. J. Prado, C. Trallero-Giner, A. M. Alcalde, V. Lopez-Richard, and G. E. Marques Phys. Rev. B **68**, 235327 (2003).
- <sup>14</sup>A. V. Fedorov, A. V. Baranov, and K. Inoue, Phys. Rev. B **54**, 8627 (1996).
- <sup>15</sup>K. I. Kang, B. P. McGinnis, Sandalphon, Y. Z. Hu, S. W. Koch, N. Peyghambarian, A. Mysyrowicz, L. C. Liu, and S. H. Risbud, Phys. Rev. B **45**, 3465 (1992).
- <sup>16</sup>D. C. Hutchings and E. W. Van Stryland, J. Opt. Soc. Am. B **9**, 2065 (1992).
- <sup>17</sup>A. I. Ekimov, F. Hache, M. C. Schanne-Klein, D. Richard, C. Flytzanis, I. A. Kudryavtsev, T. V. Yazeva, A. V. Rodina, and A. L. Efros, J. Opt. Soc. Am. B **10**, 100 (1993).
- <sup>18</sup>G. E. Tudury, M. V. Marquezini, L. G. Ferreira, L. C. Barbosa, and C. L. Cesar, Phys. Rev. B **62**, 7357 (2000).
- <sup>19</sup>L. C. Barbosa, V. C. S. Reynoso, A. M. de Paula, C. R. M. de Oliveira, O. L. Alves, A. F. Craievich, R. E. Marotti, C. H. B. Cruz, and C. L. Cesar, J. Non-Cryst. Solids **219**, 205 (1997).
- <sup>20</sup>W. W. Yu, L. H. Qu, W. Z. Guo, and X. G. Peng, Chem. Mater. **15**, 2854 (2003).
- <sup>21</sup>S. D. Bunge, K. M. Krueger, T. J. Boyle, M. A. Rodriguez, T. J. Headley, and V. L. Colvin, J. Mater. Chem. **13**, 1705 (2003).
- <sup>22</sup>L. H. Qu and X. G. Peng, J. Am. Chem. Soc. **124**, 2049 (2002).
- <sup>23</sup>M. Sheik-Bahae, A. A. Said, T. H. Wei, D. J. Hagan, and E. W. Van Stryland, IEEE J. Quantum Electron. **26**, 760 (1990).
- <sup>24</sup>C. Xu and W. W. Webb, J. Opt. Soc. Am. B **13**, 481 (1996).
- <sup>25</sup>J. M. Hales, D. J. Hagan, E. W. Van Stryland, K. J. Schafer, A. R. Morales, K. D. Belfield, P. Pacher, O. Kwon, E. Zojer, and J. L. Bredas, J. Chem. Phys. **121**, 3152 (2004).
- <sup>26</sup>R. A. Negres, J. M. Hales, A. Kobaykov, D. J. Hagan, and E. W. Van Stryland, IEEE J. Quantum Electron. **38**, 1205 (2002).
- <sup>27</sup>D. J. Norris and M. G. Bawendi, Phys. Rev. B **53**, 16338 (1996).
- <sup>28</sup>D. Ricard, Ph. Roussignol, and Chr. Flytzanis, Opt. Lett. **10**, 511 (1985).